Maltose Binding Protein Effectively Stabilizes the Partially Closed Conformation of the ATP-binding Cassette Transporter $MalFGK_2$

Jingwei Weng[1,3], Shuo Gu[2,3], Xin Gao[4], Xuhui Huang[2*], Wenning Wang[1*]

[1]Shanghai Key Laboratory of Molecular Catalysis and Innovative Materials, Department of Chemistry, and Institutes of Biomedical Sciences, Fudan University, Shanghai, P.R. China; [2]Department of Chemistry, Institute for Advance Study and School of Science, The Hong Kong University of Science and Technology, Clear Water Bay, Kowloon, Hong Kong; [4]Computer, Electrical and Mathematical Sciences and Engineering Division, King Abdullah University of Science and Technology, Thuwal, Saudi Arabia.

[3] These authors contribute equally to this work.

* Corresponding authors

Wenning Wang

E-mail: wnwang@fudan.edu.cn

Xuhui Huang

E-mail: xuhuihuang@ust.hk

Abstract

Maltose transporter $MalFGK_2$ is a Type I importer in the ATP-binding cassette (ABC) transporter superfamily. Upon the binding of its periplasmic binding protein: MalE, the ATPase activity of $MalFGK_2$ can be greatly enhanced. Crystal structures of the $MalFGK_2$-MalE-maltose complex in a so-called pretranslocation (pre-T) state with a partially closed conformation suggest that the formation of this MalE-stabilized intermediate state is a key step leading to the outward-facing catalytic state. On the contrary, cross-linking and fluorescence studies suggest that ATP binding alone is sufficient to promote the outward-facing catalytic state, doubting the role of MalE binding. To clarify the role of MalE binding and to gain a deeper understanding of molecular mechanisms of $MalFGK_2$, we calculated the free energy surfaces (FESs) related to the lateral motion in both the presence and absence of MalE using atomistic metadynamics simulations. The results show that in the absence of MalE, laterally closing motion is energetically forbidden, but upon MalE binding, more closed conformations similar to the pre-T state become more stable. The significant effect of MalE binding on the free energy landscapes is in agreement with crystallographic studies and confirms the important role of MalE in stabilizing the pre-T state. Our simulations also reveal that the allosteric effect of MalE stimulation originates from the MalE-binding-promoted vertical motion between MalF and MalG cores, which was further supported by MD simulation of the MalE-independent mutant MalF500.

Author Summary

ABC importers are membrane proteins that utilize the energy of ATP hydrolysis to transport substances into cell. All ABC importers require a cognate periplasmic binding protein to facilitate substrate import and to stimulate ATPase activity. However, the molecular mechanism of the stimulation effect is not fully understood. In this work, we study the stimulation effect in an ABC importer responsible for maltose uptake in *E. coli* using computational methods. By free energy calculation, we provide quantitative evidence demonstrating that the binding of the periplasmic binding protein MalE can effectively induce the importer approaching the catalytic state of ATP hydrolysis by stabilizing a high-energy intermediate state. The calculated free energy landscapes also explain and reconcile discrepancies in previous experimental studies. Moreover, our study also reveals the detailed allosteric mechanism on how MalE binding induces the conformational transition.

Introduction

ATP-binding cassette (ABC) transporters constitute the largest functional superfamily of primary active transporters in nature [1,2]. They utilize the energy of ATP hydrolysis to facilitate import or export in diverse cellular processes, including multidrug resistance [3], antigen processing [4], bacterial immunity [5], and cholesterol and lipid trafficking [6,7]. All ABC transporters share a similar architecture, consisting of two transmembrane domains (TMDs) buried in lipid bilayer and two nucleotide-binding domains (NBDs) immersed in cytosol. Crystal

structure studies have identified two major conformational states of the transporters and established an "alternating-access" mechanistic model [3,8], which proposes that ATP binding and hydrolysis drive the conformational transitions of the transporter between the two states: an outward-facing state with the substrate binding site exposed to the periplasmic or extracellular side of the membrane, and an inward-facing state with the binding site oriented towards the cytoplasm. In concert to the conformational transitions, the affinity of substrate binding site is also changed to ensure unidirectional transport: net substrate uptake for importers and net expulsion for exporters.

ABC importers were found in prokaryotes only [9]. Besides TMDs and NBDs, they need the help from an additional protein in periplasm, named as periplasmic binding protein (PBP), to achieve substrate uptake. Though PBPs vary in size of approximately 25~70 kDa, the core of PBPs is structurally conserved, consisting of two lobes connected by a hinge region [10]. The lobes may close and pack together upon substrate binding and tightly trap the substrate at their interface, known as the "Venus Fly-trap" mechanism [11]. PBPs show high affinity for their substrates and are commonly believed to function by acquiring substrates and delivering them to the TMDs of importers. Intriguingly, the association of PBP with the periplasmic side of TMDs could evidently stimulate ATPase activity [12-15], though the mechanism of this effect is not fully understood.

$MalFGK_2$ is one of the best studied ABC importers, serving to uptake maltose/maltodextrins (maltooligosaccharides up to seven glucose units long) in

Escherichia coli. Crystallographic studies have revealed several conformational states of $MalFGK_2$ [16-19]. The heterodimeric TMDs are composed of MalF and MalG subunits (Fig. 1A and 1B), whose core transmembrane helices (TMHs) (TMH4-8 of MalF and TMH2-6 of MalG) enclose the substrate binding site in the middle of membrane [19,20]. In cytoplasm, each MalK subunit contains one NBD plus a regulation domain. Two nucleotide binding sites are formed at the NBD dimer interface, each composed of the highly conserved Walker A motif and the LSGGQ signature motif on the opposing NBD [21]. The crystal structures of the cognate PBP (called MalE), with or without substrate, have been solved [22,23]. As an excellent archetype of the "alternating-access" model, both major states of $MalFGK_2$ are clearly identified by crystallographic [17,19] and electron paramagnetic resonance (EPR) experiments [24-27]. These states appear in a nucleotide-dependent manner. The inward-facing state (also called the resting state) emerges in the absence of nucleotides and MalE, with the NBD dimer interface widely opened [17], whereas the outward-facing state often accompanies the binding of ATP or its mimics at the fully closed NBD dimer interface [18,19,21].

Figure 1. (A) The simulation box with the $MalFGK_2$-MalE complex buried in the palmitoyloleoylphosphatidylethanolamine (POPE) bilayer. The proteins are represented as cartoon mode. The subunits MalF, MalG, $MalK^A$ amd $MalK^B$ are colored in green, blue, orange and light orange, respectively, and MalE is in magenta. The maltose molecule is represented by VDW mode and colored in yellow. The lipid

molecules are colored in red and are represented as balls and bonds standing for the head groups and the hydrophobic tails, respectively. Some lipid molecules are removed for the sake of clarity. (B) The collective variables evaluating the lateral motion: the distance between the mass centers of MalF core and MalG core (CV^{TMD}) and the distance between the mass centers of NBDs (CV^{NBD}). The mass centers are denoted as silver and black balls and the CVs are denoted as silver and black bonds for TMD and NBD, respectively. The corresponding values of the variables in the crystal structures are marked. The large periplasmic loop 2 of MalF is removed from the figure for the sake of clarity.

The binding of MalE has been shown to play an important role in stimulating the ATPase activity of $MalFGK_2$ in various studies. In particular, the addition of MalE evidently increases the rates of ATP hydrolysis and maltose transport [12,28-30]. In 2008, Shilton *et al.* proposed that there exists a significant energy barrier between the inward-facing resting state and the outward-facing state, preventing conformational transition and ATP hydrolysis, whereas MalE binding would largely lower the energy barrier by forming a stable intermediate state and facilitate the transition to the outward-facing state [31]. Three years later, crystal structures of $MalFGK_2$ in complex with maltose-bound MalE were obtained. Relative to the resting state, the new structures show evident lateral motion resulting in partially closed NBD dimer and cytoplasmic side of TMDs [32], precisely acting as the intermediate conformation between the resting and outward-facing states. The $MalFGK_2$-MalE complex

structures were named as the pretranslocation (pre-T) state, which supports the notion that MalE binding would stabilize a partially closed intermediate state and facilitate transition to the outward-facing state.

However, the role of MalE in enhancing $MalFGK_2$'s activity was questioned by recent crosslinking and fluorescence experiments, where it was demonstrated that ATP alone is sufficient to drive the formation of the outward-facing state without the MalE binding [33]. It was further proposed that MalE does not play an important role in the transition to the outward-facing state, but instead facilitates successive steps such as the cleavage of ATP [34]. The above discrepancy between different sets of experimental studies makes the role of MalE in stimulating $MalFGK_2$'s ATPase activity remains elusive. In particular, is the pre-T state a stable state? Does MalE binding effectively induce the laterally closing motion? These questions require further exploration of the nature of MalE stimulation effect.

In the past few years, molecular dynamics (MD) simulations have been used to study ABC transporter systems, such as revealing the coupling motion inside $MalFGK_2$ [35-37] and understanding the dynamics and conformational changes of other ABC transporters [38-45]. In this work, we aimed to clarify the effect of MalE binding on $MalFGK_2$ transporter. We performed well-tempered metadynamics simulations [46] to calculate the free energy changes induced by the lateral motion with or without MalE binding. This method has been demonstrated to have efficient sampling and reduced error in free energy calculations [47-49]. Our study shows that MalE binding at the periplasmic side of the transporter clearly facilitates laterally closing motion at the

cytoplasmic side, strongly supporting the role of MalE in stabilizing the pre-T state. This allosteric effect originates from the MalE-binding-promoted vertical motion between MalF and MalG cores, which is closely correlated with the laterally closing motion. The correlated motions were also observed in the simulation of the MalE-independent mutant MalF500.

Results

The inward-facing resting state is the only stable conformation in the apo $MalFGK_2$ system

We performed a 650-ns well-tempered metadynamics simulations [46] for the **apo** system ($MalFGK_2$ in the absence of MalE) from the resting state (PDB ID: 3FH6) [17]. In the metadynamics simulation, we applied bias potentials on two collective variables (CVs): CV^{TMD} and CV^{NBD} that can sufficiently describe the laterally opening-closing motion of $MalFGK_2$. Specifically, CV^{TMD} denotes the distance between center of mass of the MalF core and the MalG core, and CV^{NBD} denotes the distance between center of mass of two NBDs (Fig. 1B, see Methods for more details). As shown in Fig. S1, CV^{TMD} displays significantly higher correlations with the pairwise inter-residue distances locating at the cytoplasmic side (see Fig. S1F) than those near the periplasmic side (see Fig. S1B&C). This indicates that CV^{TMD} mainly reflects the cytoplasmic lateral motion of TMDs. As shown in Fig. S2, CV^{NBD} is closely correlated with the variation at the NBD dimer interface (Fig. S2). As shown in Fig. S3, the free energy difference between the resting and pre-T state remains

nearly invariable in the last 150-ns of the metadynamics simulation, indicating that our simulation has reached reasonable convergence.

As shown in Fig. 2A, the calculated projections of free energy surface (FES) onto CV^{NBD} and CV^{TMD} clearly shows that the crystal structure of the inward-facing resting state at (4.12 nm, 2.34 nm) is located near the center of a relatively wide free energy minimum centered at (4.12 nm, 2.31 nm). On the other hand, the crystal structure of the pre-T state at (3.60 nm, 2.18 nm) is located at the region with ~22.7 kcal/mol higher free energy than that of the resting state. These observations strongly suggest that the inward-facing resting state is the only stable state in the **apo** system, and the closing of either TMDs or NBDs is hindered by very steep uphill free energy gradient (Fig. 2A). Our results are also in good agreement with the structural study that shows that in the absence of MalE and nucleotides, only the inward-facing state has been crystalized [17]. Moreover, our results support the functional studies that suggest that the transition to the fully closed arrangement of outward-facing state requires the binding of ATP and/or MalE [26,33].

Figure 2. (A) 2-D free energy landscape of the **apo** system. (B) 2-D free energy landscape of the **complex** system. The orange and green circles denote the projections of resting and pre-T states on the 2-D space, respectively. The contour lines of the landscapes denoting 10, 20, 30 kcal/mol are depicted. The zero point of energy is set at the energy minimum.

MalE binding largely facilitates the laterally closing motion

The metadynamics simulation of the **complex** system ($MalFGK_2$ in complex with MalE) was also subjected to the convergence check using the same criteria as the **apo** system (see red curve in Fig. S3). MalE remained in the closed conformation throughout the simulation with a maltose molecule tightly bound inside the binding pocket. The free energy landscape of the **complex** system (Fig. 2B) shows a very different topography from that of the **apo** system (Fig. 2A). In particular, laterally opening arrangement exemplified by the resting state is no longer stable on the FES of the **complex** system, and areas with smaller CV^{TMD} values have lower energies (Fig. 2B). The global minimum shifts to (3.85 nm, 2.03 nm), which is 18.4 kcal/mol lower in free energy than the laterally opening conformations. The free energy landscape around the global minimum is quite flat. The region ranging from 3.73 to 4.10 nm along CV^{NBD} and from 2.0 to 2.16 nm along CV^{TMD} has free energy differences of less than 3.0 kcal/mol with respect to the global minimum (Fig. 2B).

Notably, the global minimum (3.85 nm, 2.03 nm) is quite different from the crystal structure of the pre-T state (3.60 nm, 2.17 nm). It is 10.0 kcal/mol lower in free energy and has a more opened NBD dimer and a more closed TMD interface. The structural deviations between the pre-T crystal structure and the global minimum structure could be attributed to various possible reasons such as crystal packing and a second MalF binding. In the crystal structure of the pre-T state, two MalK subunits are respectively in close contact with the MalE subunit and the periplasmic loop (PL) 2 of MalF in the neighboring cells [32], which may disturb the state of the NBD dimer

interface. Moreover, a second maltose molecule was identified in the substrate binding site at the MalF-MalG interface in the crystal structure of the pre-T state [32].. As this maltose was considered to be not physiological relevant due to the high concentration of maltose used in crystallization [32], we removed it in our simulations. We anticipate that its presence is likely to enlarge the space between the subunits, resulting in a more open TMD interface in the crystal structure. Despite the deviation of the global minimum from the pre-T state, the FES of the **complex** system is overall in agreement with the crystallographic results by showing that MalE binding changes the energy landscape dramatically and promotes the closing of the NBD dimer interface as well as the cytoplasmic end of the TMDs.

To further verify the above results obtained from metadynamics simulations, we performed eight independent 100-ns unbiased MD simulations initiated from an intermediate structure lying between the resting and pre-T state of the **complex** system. As shown in Fig. S4A&B, these MD trajectories travelled toward smaller CV^{TMD} and reached the free energy minimum identified by our metadynamics simulations. However, in the absence of MalE (**apo** system), most MD simulations transit toward larger CV^{TMD} and ended up in the free energy minimum corresponding to the resting state.

Relative vertical motion between MalF and MalG correlates with the laterally closing motion of the inward-facing conformation

The metadynamics and conventional MD simulations clearly demonstrate that MalE

binding induces the laterally closing motion of the resting state transporter, and promotes the transition to the pre-T state. To understand the underlying allosteric mechanism of MalE binding, we compared the crystal structures of the resting and pre-T states and found that along with the lateral motion, several segments at the periplasmic side of MalF core undergo collective downward motion relative to the MalG core, including the periplasmic ends of TMH4, TMH6 and TMH7, the C-terminal part of PL3 (between TMH5 and TMH6) and most part of PL4 (between TMH7 and TMH8) (Fig. 3A). The displacement at the contact interface between MalF and MalG is limited to only 0.2 nm, whereas the residues far from the interface could move vertically by over 0.5 nm. A close view on the MalFG-MalE interface provides further evidence for the functional necessity of the vertical motion. After overlapping the MalG core of the crystal structures of resting and pre-T states, we found that the PLs on MalF are too close to the PBP in the resting state (Fig. 3B). Obvious steric hindrance between them would prevent MalE binding. Thus, the relative vertical motion between MalF and MalG is essential to adjust the binding interface and refine the interactions between MalE and $MalFGK_2$.

Figure 3. (A) Motion vectors of the C_α atoms on MalF core (deep blue) pointing from the resting state (PDBID: 3FH6) to the pre-T state (PDBID: 3PV0) after the superimposition of MalG cores. The protein is represented by cartoon mode and $TMH8^F$ is omitted for clarity. The cones and cylinders represent the directions and lengths of the vectors, respectively. The vectors of atoms which show evident

downward motion are colored yellow and the vectors of the rest are colored red. The C_α atom of the mutated Gly338 in **MalF500** mutant is represented by a magenta ball and is pointed out by an arrow. (B) Close view of the MalFG-MalE interface. The MalG cores in the crystal structures of the resting and pre-T states are superimposed. The subunits in different structures are colored respectively. (C) Projections of the conventional MD trajectories on the 2-D space spanned by the vertical motion indicator and CV^{NBD}. Only the last 65 ns of each trajectory were used.

To quantify the above mentioned vertical motion, we defined a progress indicator, which is 0% for the resting state and 100% for the pre-T state (see Methods for details). Then the conventional MD trajectories were projected onto the 2-D space spanned by the indicator and CV^{NBD}. There is an obvious correlation between the vertical motion at the periplasmic side and the lateral motion of the NBD dimer interface in both **apo** and **complex** systems (Fig. 3C). The correlation has two important implications. First, triggering vertical motion could allosterically promote the laterally closing motion, in good accordance with the conformational changes induced by MalE binding. Second, the lateral motion would be dragged down by the cumbersome vertical motion, which involves shear movement at the MalF-MalG interface and disruption of inter-domain hydrogen bond interactions (such as those between $Lys337^F$-$Tyr252^G$ and between $Asn439^F$-$Pro132^G$).

The MalE-independent mutant MalF500 supports the correlation between the

vertical motion and the lateral motion

To further validate the mechanism of MalE stimulation effect, we turn to a "MalE-independent" mutant, MalF500, whose mutations could mimic the effect of MalE binding by closing NBD interface and sustaining maltose transportation without the presence of MalE [50,51]. One of its site mutations is G338R which is located on $PL3^{F}$ at the MalF-MalG interface (Fig. 3A) and the other mutation N505I is located on the $TMH8^{F}$ buried in the hydrophobic region of membrane [52]. We built the model structure of **MalF500** system directly from the aforementioned intermediate structure of the wild-type **apo** system and launched eight 100-ns trajectories. Though the simulation time is not long enough to attain a fully equilibrated ensemble, the **MalF500** system exhibited distinct behavior from the wild-type transporter. The distribution of CV^{NBD} shifted to smaller values, indicating evident laterally closing of the NBD dimer (Fig. 4A). At the same time, the highest peak of the vertical motion indicator shifted from 30% to 50%, close to that of the MalE-bound system (Fig. 4B). The enlargement of the side chain brought by G338R mutation may produce serious steric collision between $PL3^{F}$ and $TMH6^{G}$, pushing away the loop, and contributing to the vertical motion. Therefore, the simulations of the **MalF500** mutant further support the correlation between the vertical motion and the lateral motion and also suggest that the correlation relationship could be utilized to allosterically regulate the arrangement of NBD dimer interface.

Figure 4. (A) Distribution of the vertical motion indicator in the conventional MD simulations of the **apo**, **MalF500** and **complex** systems. (B). Distribution of CV^{NBD} in

310 the conventional MD simulations of the **apo**, **MalF500** and **complex** systems. Only
311 the last 65 ns of the 100-ns trajectories were used.
312
313 **Discussion**
314 The PBP stimulation effect is widely observed in ABC importers. For the maltose
315 transporter $MalFGK_2$, the mechanism of MalE stimulation effect has been studied for
316 decades and accumulating evidences suggest that MalE binds and stabilizes a partially
317 closed state in the middle of the conversion from the inward-facing state to the
318 outward-facing state. This model is supported by the crystal structure of the
319 MalE-associated pre-T state, which shows a partially closed conformation of the
320 transporter [32]. Some EPR experiments validate the existence of pre-T state and also
321 show that its stability depends heavily on the membrane/detergent environment [53].
322 However, this role of MalE was recently challenged by crosslinking and fluorescence
323 assay studies [33].
324 In this work, we calculated the dependence of free energy of $MalFGK_2$ on the lateral
325 opening-closing motion in the presence and absence of MalE. It turns out that the
326 inward-facing resting state is the most and the only stable state on the FES of the **apo**
327 system, while partially closed conformations are unstable and very high in energy
328 (Figure 2A). Therefore, our calculations are consistent with the EPR experimental
329 observations that in the absence of MalE, the inward-facing resting conformation is
330 very stable [26,27,53,54].
331 Upon MalE binding, however, partially closed conformations become more stable and

laterally opening of the cytoplasmic parts costs 18.4 kcal/mol relative to the global minimum on the 2-D FES (Fig. 2B). These results are in good agreement with the crystal structure of the MalE-associated pre-T state and confirm that MalE binding can remarkably stabilize the partially closed conformation. The large variation in energy also indicates that the contribution from MalE binding would be crucial for the laterally closing motions at the NBD dimer interface and the cytoplasmic side of TMDs, and supports the notion that MalE stimulation effect is conducted by stabilizing a partially closed intermediate state and facilitating the transition to the outward-facing state.

On the other hand, we note that the free energy landscape of the **complex** system is quite flat in the low energy area (Figure 2B), indicating remarkable conformational flexibility of the **complex** system. Especially, the free energy remains very low while the inter-NBD distance spans the range of 0.37 nm (Figure 2B). The conformational flexibility implicates that the transport activity of a transporter can be sensitive to membrane/detergent environment, which has been observed in many previous experimental studies [29,55,56]. Moreover, our simulation indicates that the structure of the pre-T state is deviated in the crystallographic condition. The global minimum structure of the **complex** system shows a more open NBD dimer interface, and the inter-NBD distance is only 0.27-nm smaller than that of the resting state. The remarkable flexibility and the relatively small changes at the NBD dimer interface could pose a great challenge to the resolution capability of the experimental methodologies, as the variation of inter-residue distance measured in experiments

would be quite limited during the conformational transition from the resting state to the partially closed state. This may explain why the spin labels across NBD dimer interface could hardly discriminate the changes brought by MalE binding in the absence of nucleotides [26,27,53,54], and why the BMOE crosslinker and the fluorescent dye N-(1-pyrene) maleimide failed to detect the effect of MalE binding [33].

To better understand the MalE stimulation effect, unraveling the molecular mechanism underlying this allosteric effect is essential. Our simulations reveal that a relative vertical motion between MalF and MalG cores at the periplasmic side is closely correlated with the lateral motion of NBD dimer (Fig. 3C and 4). The correlation indicates that factors facilitating the vertical displacement between the two TMDs near the periplasmic side, such as MalE association and various MalE-independent mutations, would promote the laterally closing motion of the inward-facing resting state. MalE binding forces the vertical displacement to remove steric collisions with MalFG and to form optimal interactions at their interface (Fig. 3B), whereas MalF500 mutant facilitates the vertical motion in a more delicate way (Fig. 4). It is interesting to note that all the MalE-independent mutations are found in the integral membrane domains, MalF or/and MalG, and never in MalK [52]. In the context of the allosteric mechanism revealed in this study, the mutations imply that the only effective way of activating the lateral motion is to modulate the packing between MalF and MalG directly.

It should be noted that what MalE binding facilitates is only the first step in the

transition to the outward-facing state. The successive steps would be still energy consuming, especially the large-scale rearrangements of MalF-MalG interface at the periplasmic side [19,32]. Although the outward-facing state is out of our FES due to its fully closed NBD dimer interface (CV^{NBD} = 2.89 nm), the topography of the FES suggests that it is probably very high in energy and unreachable through thermo fluctuations (Figure 2B). This is consistent with many experimental observations that ATP binding is essential for the complete conversion of the transporter to the outward-facing state [18,19,21,24,26,33,54]. Based on crosslinking and fluorescence assay experiments, Bao *et al.* proposed that ATP alone can accomplish the conversion to outward-facing state [33], however, EPR experiments found that both MalE and ATP are required for the conversion [26,27,54]. As nucleotides were not included in the simulation systems, our calculation could not directly evaluate the effect of ATP binding on the conformational transition. Further studies on nucleotide-associated systems are required to clarify this issue.

Methods

System Setup and MD Simulation Parameters

We used the GROMACS 4.5.5 [57] software and Amber99sb force field [58] in the MD simulations. The initial structure of the **complex** system ($MalFGK_2$ in complex with MalE) was obtained from the crystal structure of the pre-T state (PDBID: 3PV0). The initial structure of **apo** system ($MalFGK_2$ alone) was obtained from the crystal structure of the resting state (PDBID: 3FH6) and the missing residues were built

based on the corresponding parts of the outward-facing crystal structure (PDBID: 2R6G). The C_α atoms of MalG residues 37, 38, 75 and 76 were minimal-root-mean-square deviation (RMSD) overlapped between the two structures, and PL1 of MalG (residue 39 to 74) in the outward-facing structure was used for the **apo** system. The C_α atoms of MalG residues 279 to 284 were minimal-RMSD overlapped between the two structures, and the C-terminus of MalG (residue 284 to 296) in the outward-facing structure was used. The missing coordinates of the loop between $TMH2^F$ and $TMH3^F$ (residue 52 to 72) were obtained after overlapping MalF residues 47 to 52 and 71 to 76, and those of the MalF PL2 (residue 83 to 284) were obtained by overlapping MalF residues 77 to 88 and 262 to 269. $TMH1^F$ was truncated, as this helix does not significantly affect the folding or transport function of the transporter [59]. A 3000-step energy minimization successfully repaired the distorted backbone bonds at the connecting points and removed the possible bad contacts in the obtained structure.

A pre-equilibrated bilayer consisted of 340 palmitoyloleoylphosphatidylethanolamine (POPE) molecules described by the Slipids force field [60,61] was positioned around the TMDs of the transporter through the "shrinking" method [62]. Then the protein-bilayer complex was solvated in a triclinic box with about 47671 SPC water molecules [63] and neutralized by sodium ions. The ionized system was first minimized with the steepest descent algorithm, followed by a 200-ps NPT MD simulation with position restraints on the heavy atoms of the protein. The temperature was kept at 310 K using the velocity-rescaling thermostat [64] and the pressure was

maintained at 1 bar using semi-isotropic Parrinello-Rahman barostat [65]. The cut-offs of VDW and short-range electrostatic interactions were both set to 1.2 nm, and long-range electrostatic interactions were calculated by the Particle-Mesh Ewald method [66]. All the bonds in biomolecules were constrained by the LINCS algorithm [67] and the bonds in water molecules by the SETTLE algorithm [68]. Structural visualization was done by VMD [69].

The structure of the MalE-independent mutant MalF500 was built based on the intermediate structure of the **apo** system. Site mutations such as G338R and N505I were manually executed, followed by a 5000-step energy minimization.

Deriving the Force Field Parameters for Maltose

The same procedure [70] was followed to derive both bonded and non-bonded force field parameters for maltose. After the quantum mechanics (QM) calculations using the density functional theory and basis set of B3LYP/6-31G* in Gaussian program, we fitted the parameters in the stretching, bending and torsion terms of the potential function. The partial charges were derived from QM calculations with HF/6-31G* followed by the restrained electrostatic potential (RESP) method [71].

Metadynamics Simulations

Metadynamics was first introduced by Parrinello's group as a powerful method to determine the free energy surface of complex systems represented by several collective variables (CVs) using a history-dependent potential term [72,73]. For better

control of the convergence and errors of metadynamics simulation, we employed the well-tempered metadynamics, in which the height of added Gaussian potential is rescaled according to the history-dependent potential [46]. All metadynamics simulations in this work were performed by PLUMED plug-in version 1.3 [74] with GROMACS 4.5.5. Two CVs were defined to delineate the lateral motion at the TMD interface and at the NBD interface, respectively. CV^{TMD} evaluates the distance between the C_α mass centers of the MalF core (residue 277 to 506) and the MalG core (residue 77 to 283), and CV^{NBD} evaluates the distance between the C_α mass centers of the NBDs which are represented by every other two residues in the domains (residue 2 to 215). The sampling region was restrained within 2.0~2.5 nm for CV^{TMD} and within 3.3~4.5 nm for CV^{NBD} using restraining potentials, with an energy constant of 10000 kJ/mol, a rescaling factor of 0.01 nm, and an exponent determining the power law of 4.

Two systems (with or without MalE association) were simulated. Each system was maintained at 310 K and the simulations lasted for 650 ns. The initial Gaussian height was set to 2 kJ/mol and the bias factor was 10. The applied Gaussians in the metadynamics simulations were accumulated to obtain the 2-D free energy landscapes.

Relative Vertical Motion Analysis

The relative vertical motion between MalF and MalG are evaluated by an indicator *I* which quantifies the degree of completion of the vertical motion from the resting state

464 to the pre-T state:

465 $$I = \frac{X(t) - X_r}{\left\| X_{pt} - X_r \right\|} \cdot \frac{X_{pt} - X_r}{\left\| X_{pt} - X_r \right\|} \times 100\%$$

466 in which X_r and X_{pt} are the coordinate vectors of the C_α atoms in the selected part of
467 MalF for the resting and pre-T states, respectively, $X(t)$ is the instantaneous coordinate
468 vector of a snapshot from a trajectory and ||…|| denotes the vector length. The
469 indicator equals zero for the resting state and equals 100% for the pre-T state. The
470 residues at the periplasmic side of MalF showing evident vertical motions in the
471 crystal structures were selected for the calculation, which include Pro276 to Val298,
472 Lys337 to Gly380 and Phe434 to Phe476. The calculation was conducted after the
473 superposition of MalG core.

474

475 **Acknowledgments**

476 This work was supported by National Major Basic Research Program of China
477 (2016YFA0501702), National Science Foundation of China (21473034, 21403036),
478 Specialized Research Fund for the Doctoral Program of Higher Education
479 (20130071140004). X.H. acknowledges the Hong Kong Research Grants Council
480 (M-HKUST601/13, 609813, 16302214, 16304215, and HKUST C6009-15G). X.G.
481 thanks the support by funding from King Abdullah University of Science and
482 Technology (KAUST). This research made use of the resources of the computer
483 clusters at KAUST and the super computer center at Fudan University.

484

485

486

Reference

1. Zheng WH, Vastermark A, Shlykov MA, Reddy V, Sun EI *et al.* (2013) Evolutionary relationships of ATP-Binding Cassette (ABC) uptake porters. BMC Microbiol 13: 98.

2. George AM, Jones PM (2012) Perspectives on the structure-function of ABC transporters: the Switch and Constant Contact models. Prog Biophys Mol Biol 109: 95-107.

3. Seeger MA, van Veen HW (2009) Molecular basis of multidrug transport by ABC transporters. Biochim Biophys Acta 1794: 725-737.

4. Parcej D, Tampe R (2010) ABC proteins in antigen translocation and viral inhibition. Nat Chem Biol 6: 572-580.

5. Hinz A, Tampe R (2012) ABC transporters and immunity: mechanism of self-defense. Biochemistry 51: 4981-4989.

6. Tarling EJ, de Aguiar Vallim TQ, Edwards PA (2013) Role of ABC transporters in lipid transport and human disease. Trends Endocrinol Metab 24: 342-350.

7. Ueda K (2011) ABC proteins protect the human body and maintain optimal health. Biosci Biotechnol Biochem 75: 401-409.

8. Locher KP (2009) Review. Structure and mechanism of ATP-binding cassette transporters. Philos Trans R Soc Lond B 364: 239-245.

9. Davidson AL, Chen J (2004) ATP-binding cassette transporters in bacteria. Annu Rev Biochem 73: 241-268.

10. Berntsson RP, Smits SH, Schmitt L, Slotboom DJ, Poolman B (2010) A structural classification of substrate-binding proteins. FEBS Lett 584: 2606-2617.

510 11. Mao B, Pear MR, McCammon JA, Quiocho FA (1982) Hinge-bending in
511 L-arabinose-binding protein. The "Venus's-flytrap" model. J Biol Chem 257:
512 1131-1133.
513 12. Davidson AL, Shuman HA, Nikaido H (1992) Mechanism of maltose transport in
514 Escherichia coli: transmembrane signaling by periplasmic binding proteins. Proc Natl
515 Acad Sci U S A 89: 2360-2364.
516 13. Liu CE, Liu PQ, Ames GF (1997) Characterization of the adenosine
517 triphosphatase activity of the periplasmic histidine permease, a traffic ATPase (ABC
518 transporter). J Biol Chem 272: 21883-21891.
519 14. Borths EL, Poolman B, Hvorup RN, Locher KP, Rees DC (2005) In vitro
520 functional characterization of BtuCD-F, the Escherichia coli ABC transporter for
521 vitamin B12 uptake. Biochemistry 44: 16301-16309.
522 15. Tal N, Ovcharenko E, Lewinson O (2013) A single intact ATPase site of the ABC
523 transporter BtuCD drives 5% transport activity yet supports full in vivo vitamin B12
524 utilization. Proc Natl Acad Sci U S A 110: 5434-5439.
525 16. Chen S, Oldham ML, Davidson AL, Chen J (2013) Carbon catabolite repression
526 of the maltose transporter revealed by X-ray crystallography. Nature 499: 364-368.
527 17. Khare D, Oldham ML, Orelle C, Davidson AL, Chen J (2009) Alternating access
528 in maltose transporter mediated by rigid-body rotations. Mol Cell 33: 528-536.
529 18. Oldham ML, Chen J (2011) Snapshots of the maltose transporter during ATP
530 hydrolysis. Proc Natl Acad Sci U S A 108: 15152-15156.
531 19. Oldham ML, Khare D, Quiocho FA, Davidson AL, Chen J (2007) Crystal

532 structure of a catalytic intermediate of the maltose transporter. Nature 450: 515-521.
533 20. Oldham ML, Chen S, Chen J (2013) Structural basis for substrate specificity in
534 the Escherichia coli maltose transport system. Proc Natl Acad Sci U S A 110:
535 18132-18137.
536 21. Chen J, Lu G, Lin J, Davidson AL, Quiocho FA (2003) A tweezers-like motion of
537 the ATP-binding cassette dimer in an ABC transport cycle. Mol Cell 12: 651-661.
538 22. Spurlino JC, Lu GY, Quiocho FA (1991) The 2.3-A resolution structure of the
539 maltose- or maltodextrin-binding protein, a primary receptor of bacterial active
540 transport and chemotaxis. J Biol Chem 266: 5202-5219.
541 23. Sharff AJ, Rodseth LE, Spurlino JC, Quiocho FA (1992) Crystallographic
542 evidence of a large ligand-induced hinge-twist motion between the two domains of
543 the maltodextrin binding protein involved in active transport and chemotaxis.
544 Biochemistry 31: 10657-10663.
545 24. Grote M, Bordignon E, Polyhach Y, Jeschke G, Steinhoff HJ *et al.* (2008) A
546 comparative electron paramagnetic resonance study of the nucleotide-binding
547 domains' catalytic cycle in the assembled maltose ATP-binding cassette importer.
548 Biophys J 95: 2924-2938.
549 25. Grote M, Polyhach Y, Jeschke G, Steinhoff HJ, Schneider E *et al.* (2009)
550 Transmembrane signaling in the maltose ABC transporter MalFGK2-E: periplasmic
551 MalF-P2 loop communicates substrate availability to the ATP-bound MalK dimer. J
552 Biol Chem 284: 17521-17526.
553 26. Orelle C, Ayvaz T, Everly RM, Klug CS, Davidson AL (2008) Both

554 maltose-binding protein and ATP are required for nucleotide-binding domain closure
555 in the intact maltose ABC transporter. Proc Natl Acad Sci U S A 105: 12837-12842.
556 27. Orelle C, Alvarez FJ, Oldham ML, Orelle A, Wiley TE *et al.* (2010) Dynamics of
557 alpha-helical subdomain rotation in the intact maltose ATP-binding cassette
558 transporter. Proc Natl Acad Sci U S A 107: 20293-20298.
559 28. Reich-Slotky R, Panagiotidis C, Reyes M, Shuman HA (2000) The
560 detergent-soluble maltose transporter is activated by maltose binding protein and
561 verapamil. J Bacteriol 182: 993-1000.
562 29. Bao H, Duong F (2012) Discovery of an auto-regulation mechanism for the
563 maltose ABC transporter MalFGK2. PloS One 7: e34836.
564 30. Shilton BH (2015) Active transporters as enzymes: an energetic framework
565 applied to major facilitator superfamily and ABC importer systems. Biochem J 467:
566 193-199.
567 31. Shilton BH (2008) The dynamics of the MBP-MalFGK(2) interaction: a prototype
568 for binding protein dependent ABC-transporter systems. Biochim Biophys Acta 1778:
569 1772-1780.
570 32. Oldham ML, Chen J (2011) Crystal structure of the maltose transporter in a
571 pretranslocation intermediate state. Science 332: 1202-1205.
572 33. Bao H, Duong F (2013) ATP alone triggers the outward facing conformation of
573 the maltose ATP-binding cassette transporter. J Biol Chem 288: 3439-3448.
574 34. Bao H, Dalal K, Cytrynbaum E, Duong F (2015) Sequential Action of MalE and
575 Maltose Allows Coupling ATP Hydrolysis to Translocation in the MalFGK2

576 Transporter. J Biol Chem 290: 25452-25460.
577 35. Oliveira AS, Baptista AM, Soares CM (2011) Inter-domain communication
578 mechanisms in an ABC importer: a molecular dynamics study of the MalFGK2E
579 complex. PLoS Comput Biol 7: e1002128.
580 36. Wen PC, Tajkhorshid E (2011) Conformational coupling of the nucleotide-binding
581 and the transmembrane domains in ABC transporters. Biophys J 101: 680-690.
582 37. Li CH, Yang YX, Su JG, Liu B, Tan JJ *et al.* (2014) Allosteric transitions of the
583 maltose transporter studied by an elastic network model. Biopolymers 101: 758-768.
584 38. Aittoniemi J, de Wet H, Ashcroft FM, Sansom MS (2010) Asymmetric switching
585 in a homodimeric ABC transporter: a simulation study. PLoS Comput Biol 6:
586 e1000762.
587 39. Becker JP, Van Bambeke F, Tulkens PM, Prevost M (2010) Dynamics and
588 structural changes induced by ATP binding in SAV1866, a bacterial ABC exporter. J
589 Phys Chem B 114: 15948-15957.
590 40. Ferreira RJ, Ferreira MJU, dos Santos D (2012) Insights on P-Glycoprotein's
591 Efflux Mechanism Obtained by Molecular Dynamics Simulations. J Chem Theo
592 Comput 8: 1853-1864.
593 41. Furukawa-Hagiya T, Furuta T, Chiba S, Sohma Y, Sakurai M (2013) The power
594 stroke driven by ATP binding in CFTR as studied by molecular dynamics simulations.
595 J Phys Chem B 117: 83-93.
596 42. Jones PM, George AM (2011) Molecular-dynamics simulations of the ATP/apo
597 state of a multidrug ATP-binding cassette transporter provide a structural and

598 mechanistic basis for the asymmetric occluded state. Biophys J 100: 3025-3034.
599 43. Kandt C, Tieleman DP (2010) Holo-BtuF stabilizes the open conformation of the
600 vitamin B12 ABC transporter BtuCD. Proteins 78: 738-753.
601 44. St-Pierre JF, Bunker A, Rog T, Karttunen M, Mousseau N (2012) Molecular
602 dynamics simulations of the bacterial ABC transporter SAV1866 in the closed form. J
603 Phys Chem B 116: 2934-2942.
604 45. Wen PC, Verhalen B, Wilkens S, McHaourab HS, Tajkhorshid E (2013) On the
605 origin of large flexibility of P-glycoprotein in the inward-facing state. J Biol Chem
606 288: 19211-19220.
607 46. Barducci A, Bussi G, Parrinello M (2008) Well-tempered metadynamics: A
608 smoothly converging and tunable free-energy method. Phys Rev Lett 100: 020603.
609 47. Formoso E, Limongelli V, Parrinello M (2015) Energetics and structural
610 characterization of the large-scale functional motion of adenylate kinase. Sci Rep 5:
611 8425.
612 48. Marti-Solano M, Sanz F, Pastor M, Selent J (2014) A dynamic view of molecular
613 switch behavior at serotonin receptors: implications for functional selectivity. PloS
614 One 9: e109312.
615 49. Botten D, Fugallo G, Fraternali F, Molteni C (2013) A computational exploration
616 of the interactions of the green tea polyphenol (-)-Epigallocatechin 3-Gallate with
617 cardiac muscle troponin C. PloS One 8: e70556.
618 50. Treptow NA, Shuman HA (1985) GENETIC-EVIDENCE FOR SUBSTRATE
619 AND PERIPLASMIC-BINDING-PROTEIN RECOGNITION BY THE MALF AND

620 MALG PROTEINS, CYTOPLASMIC MEMBRANE-COMPONENTS OF THE
621 ESCHERICHIA-COLI MALTOSE TRANSPORT-SYSTEM. J Bacteriol 163:
622 654-660.
623 51. Shuman HA (1982) Active transport of maltose in Escherichia coli K12. Role of
624 the periplasmic maltose-binding protein and evidence for a substrate recognition site
625 in the cytoplasmic membrane. J Biol Chem 257: 5455-5461.
626 52. Covitz KMY, Panagiotidis CH, Hor LI, Reyes M, Treptow NA *et al.* (1994)
627 Mutations That Alter the Transmembrane Signaling Pathway in an Atp Binding
628 Cassette (ABC) Transporter. EMBO J 13: 1752-1759.
629 53. Alvarez FJ, Orelle C, Huang Y, Bajaj R, Everly RM *et al.* (2015) Full engagement
630 of liganded maltose-binding protein stabilizes a semi-open ATP-binding cassette
631 dimer in the maltose transporter. Mol Microbiol 98: 878-894.
632 54. Bohm S, Licht A, Wuttge S, Schneider E, Bordignon E (2013) Conformational
633 plasticity of the type I maltose ABC importer. Proc Natl Acad Sci U S A 110:
634 5492-5497.
635 55. Reich-Slotky R, Panagiotidis C, Reyes M, Shuman HA (2000) The
636 detergent-soluble maltose transporter is activated by maltose binding protein and
637 verapamil. J Bacteriol 182: 993-1000.
638 56. Bao H, Dalal K, Wang V, Rouiller I, Duong F (2013) The maltose ABC
639 transporter: action of membrane lipids on the transporter stability, coupling and
640 ATPase activity. Biochim Biophys Acta 1828: 1723-1730.
641 57. Hess B, Kutzner C, van der Spoel D, Lindahl E (2008) GROMACS 4: Algorithms

642 for highly efficient, load-balanced, and scalable molecular simulation. J Chem Theory
643 Comput 4: 435-447.
644 58. Hornak V, Abel R, Okur A, Strockbine B, Roitberg A *et al.* (2006) Comparison of
645 multiple amber force fields and development of improved protein backbone
646 parameters. Proteins 65: 712-725.
647 59. Ehrmann M, Beckwith J (1991) Proper insertion of a complex membrane protein
648 in the absence of its amino-terminal export signal. J Biol Chem 266: 16530-16533.
649 60. Jambeck JP, Lyubartsev AP (2012) Derivation and systematic validation of a
650 refined all-atom force field for phosphatidylcholine lipids. J Phys Chem B 116:
651 3164-3179.
652 61. Jambeck JPM, Lyubartsev AP (2012) An Extension and Further Validation of an
653 All-Atomistic Force Field for Biological Membranes. J Chem Theory Comput 8:
654 2938-2948.
655 62. Kandt C, Ash WL, Tieleman DP (2007) Setting up and running molecular
656 dynamics simulations of membrane proteins. Methods 41: 475-488.
657 63. Berendsen HJC, Grigera JR, Straatsma TP (1987) The Missing Term in Effective
658 Pair Potentials. J Phys Chem 91: 6269-6271.
659 64. Bussi G, Donadio D, Parrinello M (2007) Canonical sampling through velocity
660 rescaling. J Chem Phys 126: 014101.
661 65. Parrinello M, Rahman A (1981) Polymorphic Transitions in Single-Crystals - a
662 New Molecular-Dynamics Method. J Appl Phys 52: 7182-7190.
663 66. Cerutti DS, Duke RE, Darden TA, Lybrand TP (2009) Staggered Mesh Ewald: An

664 Extension of the Smooth Particle-Mesh Ewald Method Adding Great Versatility. J
665 Chem Theory Comput 5: 2322-2338.
666 67. Hess B, Bekker H, Berendsen HJC, Fraaije JGEM (1997) LINCS: A linear
667 constraint solver for molecular simulations. J Comput Chem 18: 1463-1472.
668 68. Miyamoto S, Kollman PA (1992) Settle - an Analytical Version of the Shake and
669 Rattle Algorithm for Rigid Water Models. J Comput Chem 13: 952-962.
670 69. Humphrey W, Dalke A, Schulten K (1996) VMD: Visual molecular dynamics. J
671 Mol Graph 14: 33-38.
672 70. Zhang L, Silva DA, Yan YJ, Huang XH (2012) Force field development for
673 cofactors in the photosystem II. J Comput Chem 33: 1969-1980.
674 71. Fuller JC, Jackson RM, Edwards TA, Wilson AJ, Shirts MR (2012) Modeling of
675 Arylamide Helix Mimetics in the p53 Peptide Binding Site of hDM2 Suggests Parallel
676 and Anti-Parallel Conformations Are Both Stable. Plos One 7: e43253
677 72. Laio A, Parrinello M (2002) Escaping free-energy minima. Proc Natl Acad Sci U
678 S A 99: 12562-12566.
679 73. Bussi G, Laio A, Parrinello M (2006) Equilibrium free energies from
680 nonequilibrium metadynamics. Phys Rev Lett 96: 090601.
681 74. Bonomi M, Branduardi D, Bussi G, Camilloni C, Provasi D *et al.* (2009)
682 PLUMED: A portable plugin for free-energy calculations with molecular dynamics.
683 Comput Phys Commun 180: 1961-1972.
684

Figure 1

Click here to download Figure Fig1.tif

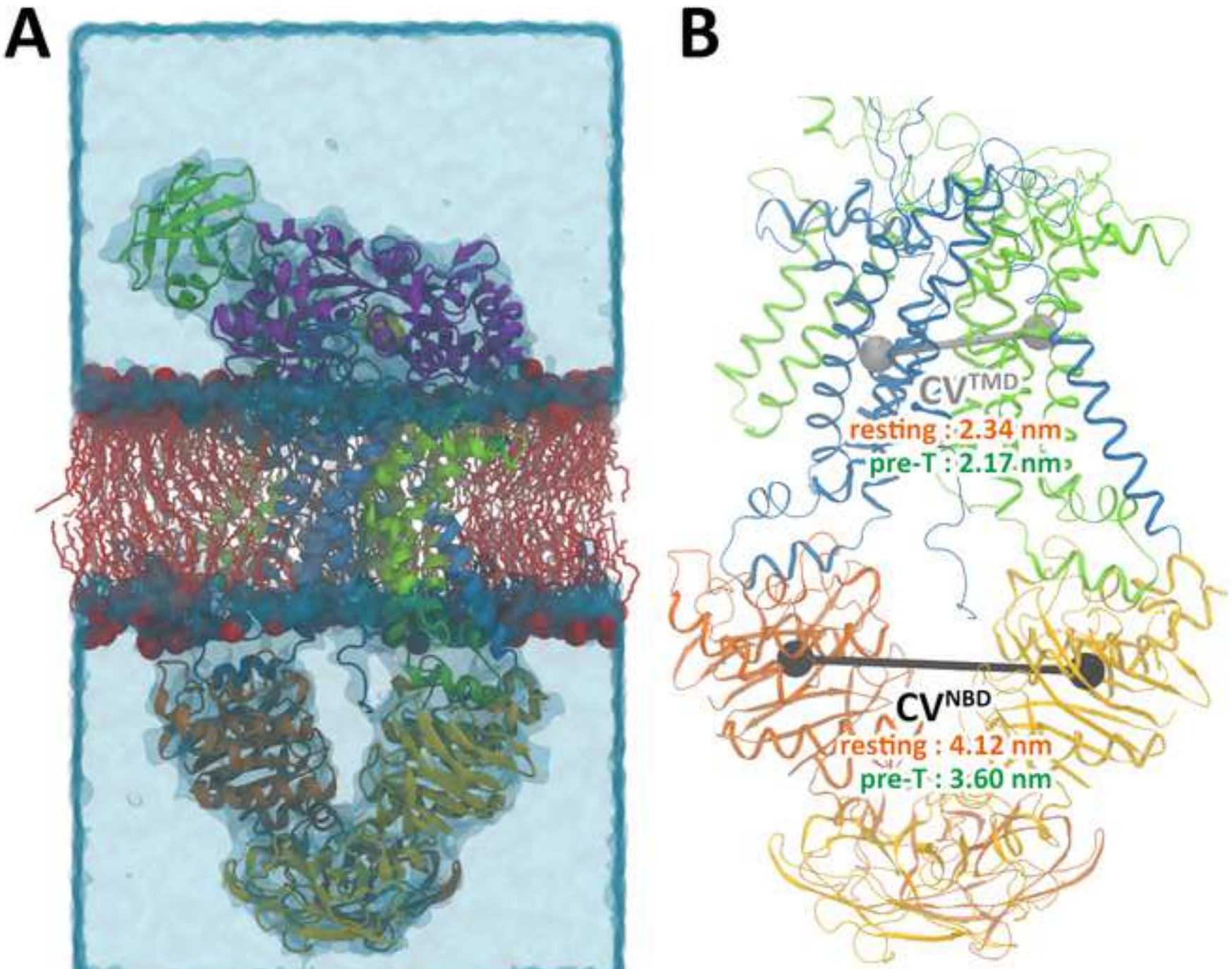

Figure 2

Click here to download Figure Fig2.tif

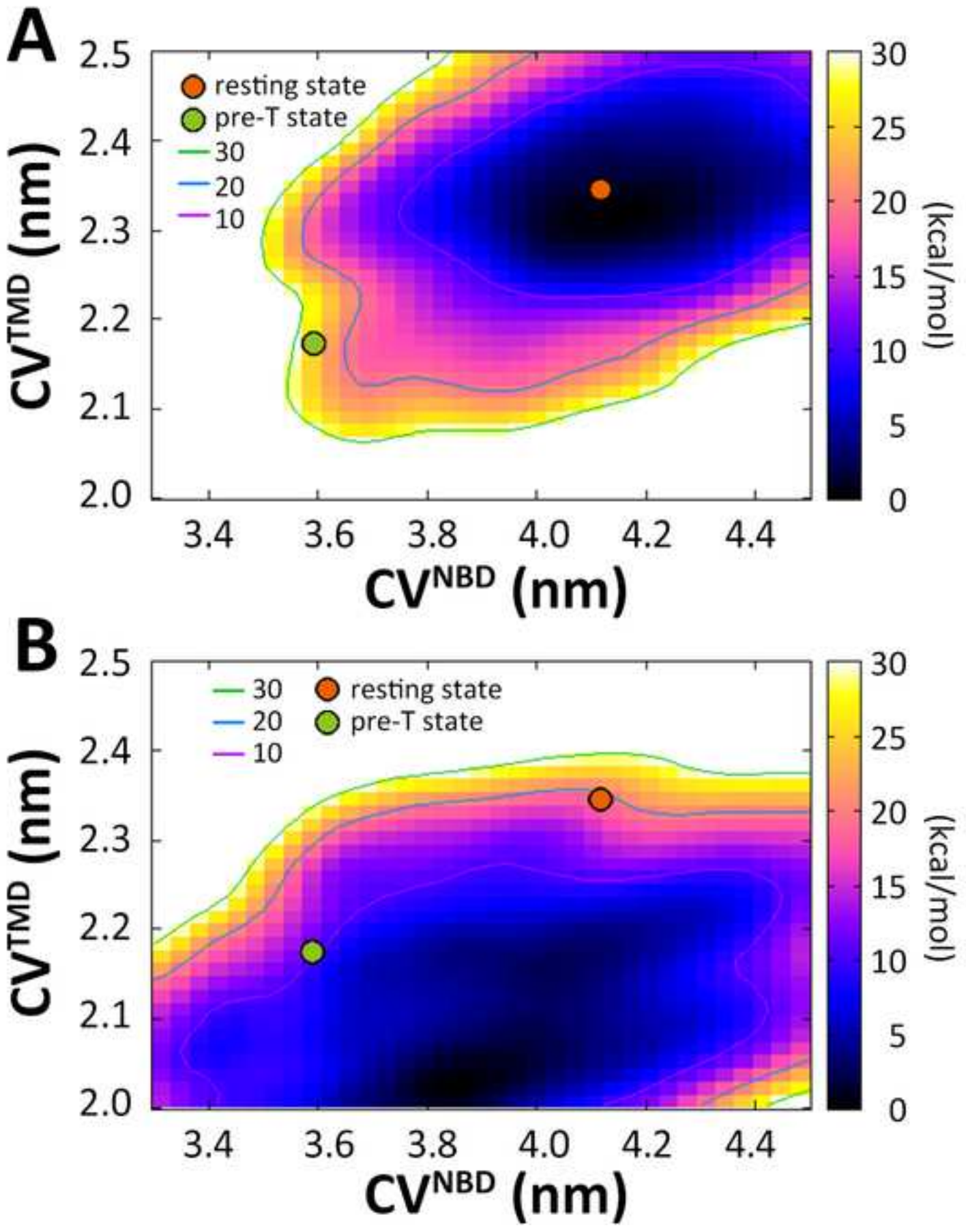

Figure 3

Click here to download Figure Fig3.tif

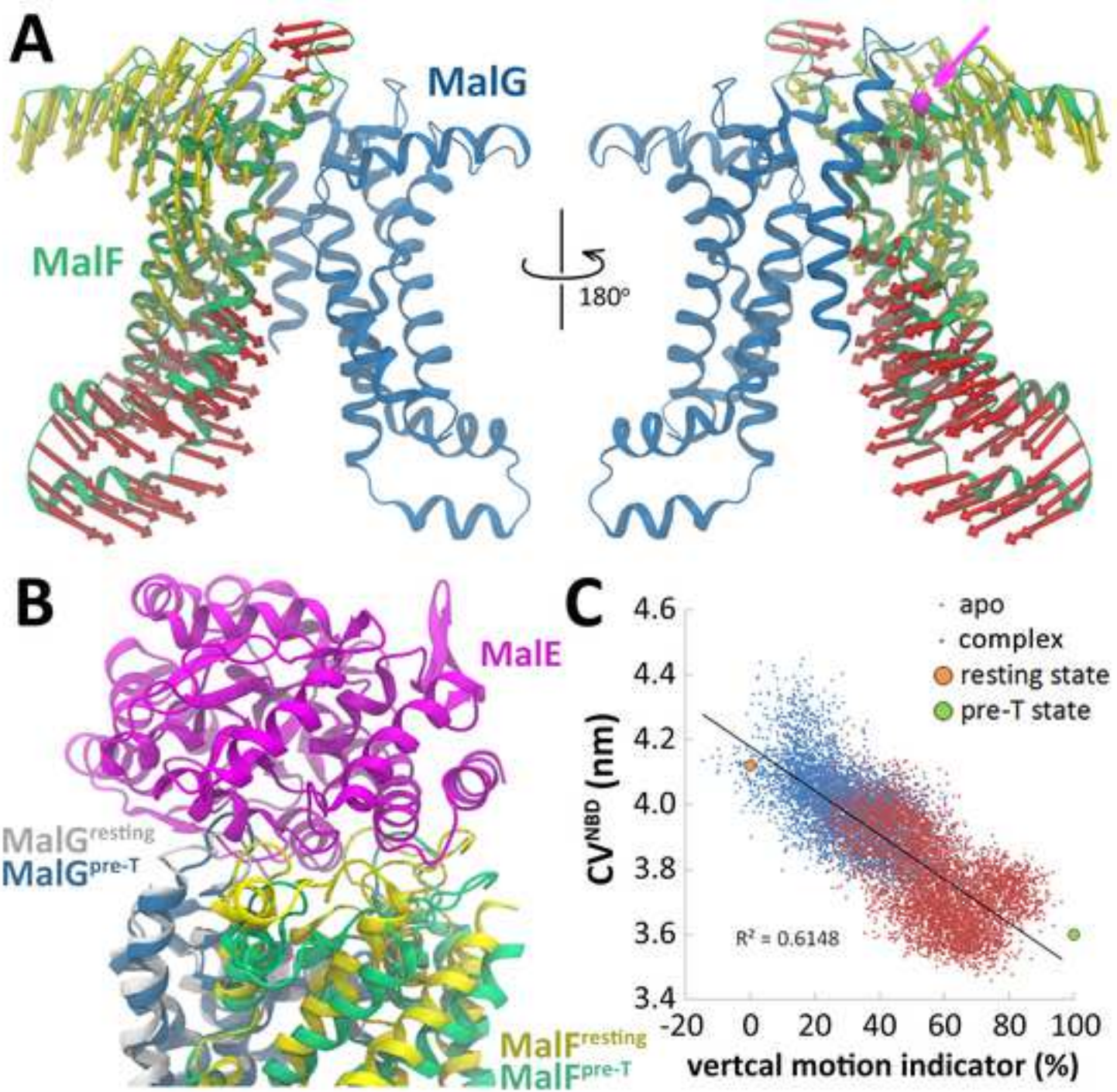

Figure 4

Click here to download Figure Fig4.tif